ACS APPLIED MATERIALS & INTERFACES

Research Article

www.acsami.org

Synthesis of Mesoporous Silica@Co–Al Layered Double Hydroxide Spheres: Layer-by-Layer Method and Their Effects on the Flame Retardancy of Epoxy Resins

Shu-Dong Jiang,[†] Zhi-Man Bai,[†,‡] Gang Tang,[†] Lei Song,[†] Anna A Stec,[§] T. Richard Hull,[§] Yuan Hu,*[,†,‡] and Wei-Zhao Hu[†]

[†]State Key Laboratory of Fire Science, University of Science and Technology of China, 96 Jinzhai Road, Hefei, Anhui 230026, China

[‡]Suzhou Key Laboratory of Urban Public Safety, Suzhou Institute for Advanced Study, University of Science and Technology of China, 166 Ren'ai Road, Suzhou, Jiangsu 215123, China

[§]Centre for Fire and Hazards Science, University of Central Lancashire, Preston PR1 2HE, United Kingdom

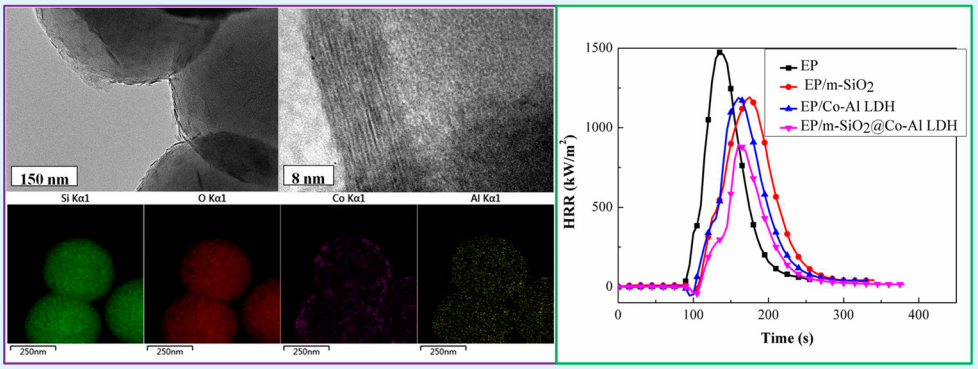

ABSTRACT: Hierarchical mesoporous silica@Co–Al layered double hydroxide (m-SiO_2@Co–Al LDH) spheres were prepared through a layer-by-layer assembly process, in order to integrate their excellent physical and chemical functionalities. TEM results depicted that, due to the electrostatic potential difference between m-SiO_2 and Co–Al LDH, the synthetic m-SiO_2@Co–Al LDH hybrids exhibited that m-SiO_2 spheres were packaged by the Co–Al LDH nanosheets. Subsequently, the m-SiO_2@Co–Al LDH spheres were incorporated into epoxy resin (EP) to prepare specimens for investigation of their flame-retardant performance. Cone results indicated that m-SiO_2@Co–Al LDH incorporated obviously improved fire retardant of EP. A plausible mechanism of fire retardant was hypothesized based on the analyses of thermal conductivity, char residues, and pyrolysis fragments. Labyrinth effect of m-SiO_2 and formation of graphitized carbon char catalyzed by Co–Al LDH play pivotal roles in the flame retardance enhancement.

KEYWORDS: *mesoporous silica@Co–Al layered double hydroxide spheres, layer-by-layer method, polymer composites, thermal stability, flame retardancy, mechanism*

1. INTRODUCTION

Mesoporous silica (m-SiO_2) has attracted much interest for its widespread applications in molecular adsorption, catalysis, gas, and biological sensors, due to its high surface area, tunable pore size and very narrow pore size distribution.[1−3] The large-area and open-pore surface of m-SiO_2 is suited to anchoring particles, trapping molecules, fast transport, and optical manipulation.[3−6] To date, m-SiO_2 has been further used to fabricate polymer nanocomposites with more excellent performance.[7−9] Compared to other reported inorganic fillers,[10−13] m-SiO_2 shows obvious advantages. On one hand, the mesopore sizes are much larger than the width of EP (about 0.5 nm). Therefore, EP can be easily penetrated into the mesochannels due to capillary force. Also, EP wrapped by the surface of m-SiO_2 exhibits high thermal stability. On the other hand, unlike nanosheets and nanotubes, the one-dimensional mesopore space is randomly oriented inside the composites to endow isotropy for nanocomposites.[14] Although m-SiO_2 is clearly a promising polymer additive, few studies have reported the new application of m-SiO_2 on the flame retardancy of polymers.[15] Thus, broadening the application of m-SiO_2 is a promising avenue of research.

As a kind of important lamellar materials, layered double hydroxides are currently obtained intense research interest owning to their excellent physical and chemical properties, which result in their extensive applications in catalysis, adsorption, and flame retardant.[16−19] However, the use of layered double hydroxides alone remains unsatisfactory to meet

Received: May 30, 2014
Accepted: July 25, 2014
Published: July 25, 2014

specific requirements for applications. Recently, core−shell structured hybrids have received tremendous attention in recent research for the combined characteristics of cores and shells. Shao et al. provided a novel Fe_3O_4@SiO_2@NiAl-LDH for the practical purification of recombinant proteins.[20] Silica microspheres decorated with CdS nanocrystals were prepared through a facile method and applied to the physical adsorption and direct photolysis of N-containing dyes.[21] Teng et al. reported the fabrication of Fe_3O_4@SiO_2 with superparamagnetism, high magnetization, and large surface area.[22] Inspired by these, this study aims to combine of m-SiO_2 and Co−Al layered double hydroxide (Co−Al LDH) to improve their flame retardancy effectiveness. Co−Al LDH is a well-investigated member of the LDH family due to its ease of synthesis and delamination.[23] The exfoliated single sheets of Co−Al layered double hydroxide (Co−Al LDH) is positively charged with a thickness of 0.8 nm.[24] It is known that the surface of m-SiO_2 is negatively charged above the isoelectric point, which favors a layer coating of the positively charged material.[25] Electrostatic interactions between negatively charged m-SiO_2 and positively charged LDH sheets can create layered structures on the surface of m-SiO_2 through a layer-by-layer assembly method.

EP is one of the most widely exploited reactive polymeric resins in laminating, adhesive, coating, and casting fields.[26,27] However, its high flammability greatly restricted its application in some areas. Herein, m-SiO_2@Co−Al LDH spheres were synthesized by ultrasound assisted direct layered assembly of Co−Al LDH nanosheets on the surface of m-SiO_2 spheres, as schematically depicted in Scheme 1. Subsequently, the m-

Scheme 1. Synthetic Route of m-SiO_2@Co−Al LDH

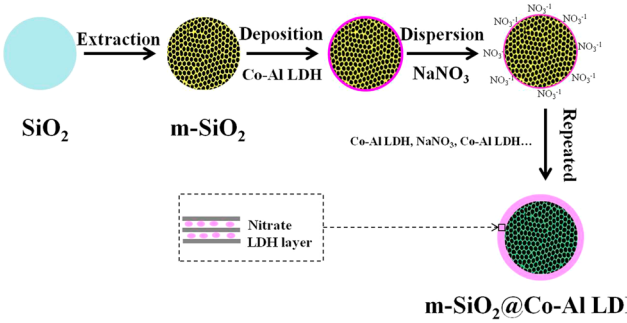

SiO_2@Co−Al LDH spheres were incorporated into an EP matrix to prepare specimens for investigation of their flame-retardant performance. The synergistic effect between m-SiO_2 and Co−Al LDH on the thermal stability and flame retardance of the as-prepared nanocomposite was systematically investigated using thermogravimetric analysis (TGA) and cone calorimeter. Meanwhile, the analyses of thermal conductivity, char residue, and pyrolysis fragments were utilized in an attempt to gain insight into flame-retardant mechanism.

2. EXPERIMENTAL SECTION

Tetraethyl orthosilicate (TEOS, AR), cetyltrimethylammonium bromide (CTAB, AR), ammonium hydroxide (28%, AR), ethanol (AR), $Co(NO_3)_2{\cdot}6H_2O$ (AR), $Al(NO_3)_3{\cdot}9H_2O$ (AR), $NaNO_3$ (AR), tetrahydrofuran (THF, AR), and 4,4′-diaminodiphenylmethane (DDM, AR) were purchased from Sinopharm Chemical Reagent Co., Ltd. (Shanghai, China). Bisphenol-A type epoxy resin was provided by shixian Chemical Industry Co., Ltd. (Guangzhou, China).

2.1. Preparation of m-SiO_2. m-SiO_2 spheres were synthesized through a modified Stöber method. In a typical synthetic process, CTAB was dissolved in ethanol aqueous solution including ammonium hydroxide. Then, TEOS (1 mL) was quickly injected into the above solution at 45 °C under strong mechanical stirring at a speed of 1500 rpm. The reactant molar ratio was 1.00 TEOS/0.0954 CTAB/2.84 NH_3/723 H_2O/125 C_2H_5OH. After 24 h of thermostatic reaction, the white precipitate was isolated by centrifugation (5000 rpm, 10 min) and cleaned by three cycles of centrifugation/washing/redispersion in ethanol. The yield of the final product was about 70%.

2.2. Preparation of Co−Al LDH. Co−Al LDH was prepared by a slow coprecipitation followed by ultrasound treatment. Briefly, 0.8 mL of aqueous ammonia solution (12.3 mmol) was added into 20 mL of deionized water to form solution A. Then, 19.2 mL of an aqueous solution containing 0.96 mmol of $Co(NO_3)_2{\cdot}6H_2O$ and 0.48 mmol of $Al(NO_3)_3{\cdot}9H_2O$ was dropped at a constant rate of 40 mL/h into solution A under vigorous mechanical stirring with a speed of 2000 rpm (JJ-1 motor stirrer, 60W, 3000 rpm, Changzhou saipu Instruments Equipment Co., Ltd., China) followed by ultrasonication for 1 h. For the ultrasonication, this was done with a typical immersion bath. The model sonic bath was KQ-250 with a frequency of 40 kHz (Gongyi Yuhua Instruments Equipment Co., Ltd., China).The obtained solid was collected and washed with pure water and ethanol. The yield of the Co−Al LDH was about 80%

2.3. Preparation of m-SiO_2@Co−Al LDH through the Layer-by-Layer Method. m-SiO_2 (0.5 g) was dispersed in a Co−Al LDH formamide solution (0.1 g/100 mL). Then, the mixture was ultrasonically agitated for 20 min to facilitate the adsorption of Co−Al LDH nanosheets onto the m-SiO_2 surface. The particles were separated by centrifugation at 6000 rpm for 10 min and washed with deionized water. In the next step, the particles were dispersed in a $NaNO_3$ solution (100 mL, 2 g/L). The pink precipitate was isolated by centrifugation (6000 rpm, 10 min). m-SiO_2 coated with 10 layer pairs of nitrate and LDH nanosheets $(NO_3^{-1}/LDH)_{10}$ were prepared through repeating the above procedures 10 times. The yield of the final product was about 90%.

2.4. Preparation of EP/m-SiO_2@Co−Al LDH Composite. A typical preparation of epoxy composite containing 2 wt % m-SiO_2@Co−Al LDH is illustrated below: m-SiO_2@Co−Al LDH (0.2 g) was added in a THF solution with ultrasonication (Immersion sonic bath, KQ-250, 40 kHz, Gongyi yuhua Instruments Equipment Co., Ltd., China) to form a pink suspension. Then, DDM (1.6 g) was melt at 95 °C and mixed with epoxy resin (8.2 g) by hand with a spatula for 10 min. Subsequently, the mixture of epoxy resin and DDM was poured into the above suspension under magnetic stirring with a speed of 1000 rpm for 30 min until a homogeneous mixture was formed. The mixture was placed in a vacuum chamber at 60 °C for 12 h to remove THF. Finally, the EP/m-SiO_2@Co−Al LDH composite was cured at 100 °C for 2 h and post cured at 150 °C for 2 h. After curing, the composite was permitted to cool to room temperature. For the preparation of neat EP, EP/Co−Al LDH, and EP/m-SiO_2 composites, an analogous prepared procedure was adopted except the variation of the additives.

2.5. Characterization. Powder X-ray diffraction (XRD) measurements were performed on a Japan Rigaku DMax/rA rotating anode X-ray diffractometer, using Cu Kα radiation (λ = 0.154 nm) at 40 kV. Transmission electron microscopy (TEM), Energy dispersive X-ray spectroscopy (EDX) and high-resolution transmission electron microscopy (HRTEM) analyses were carried out using a Hitachi model H-800 TEM with an accelerating voltage of 200 kV. Before measurement, samples were dispersed in ethanol followed by ultrasonication for 30 min at room temperature. The homogeneous mixtures were dripped on carbon-coated copper grids. UV−vis absorption spectra were detected by a Solid3700 (SHIMADZU) spectrometer. X-ray photoelectron spectroscopy (XPS) spectra were recorded on an ESCALAB 250 X-ray photoelectron spectrometer employing a monochromatic Al Kα X-ray source. Thermogravimetric analyses (TGA) of samples were implementing with the aid of a Q5000 thermal analyzer (TA Co., U.S.A.) at a heating speed of 20 °C min^{-1} in nitrogen atmosphere. The combustion properties of EP and EP composites were carried out on a cone calorimeter based on ASTM E1354/ISO 5660. Every specimen with the sizes of 100 × 100 × 3

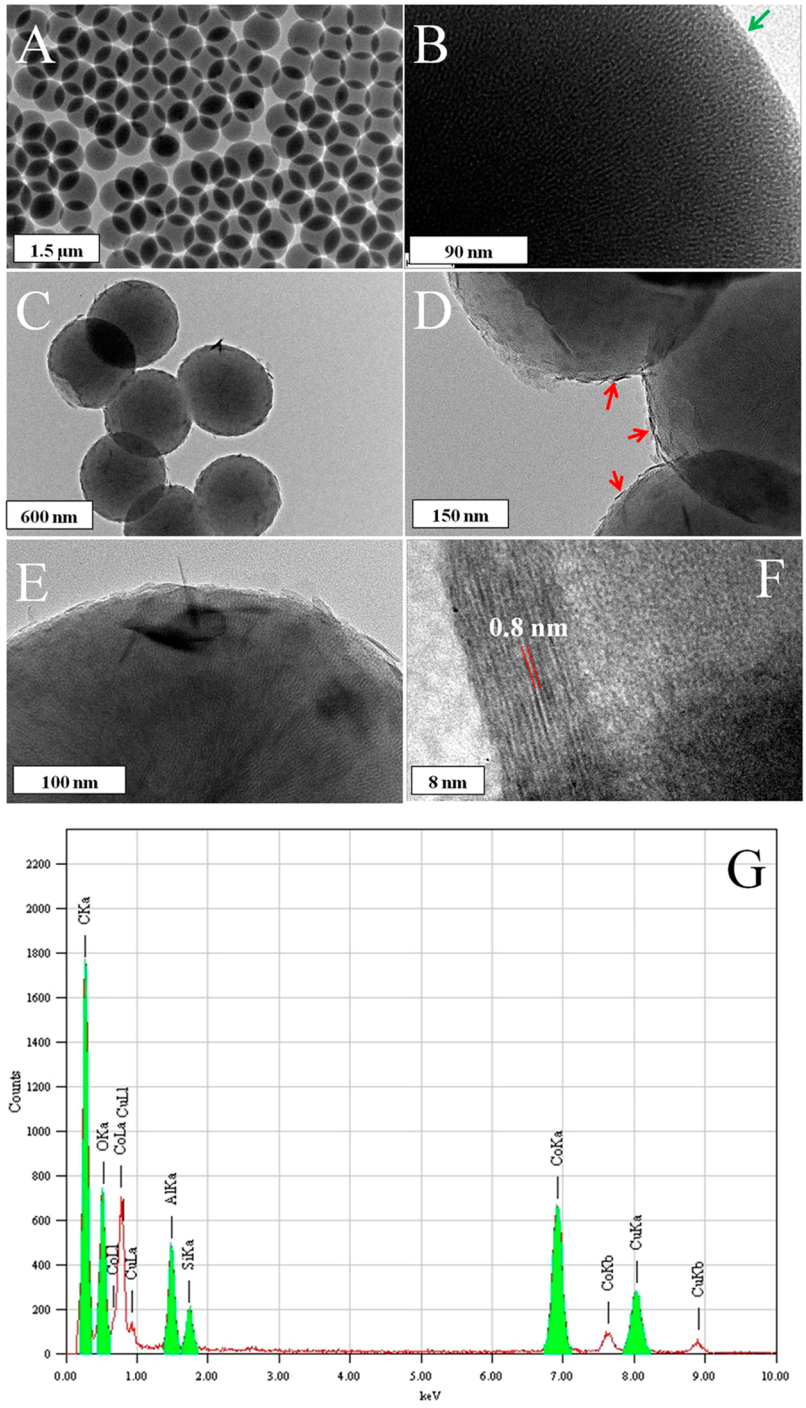

Figure 1. TEM images of m-SiO_2 (A, B), m-SiO_2@Co−Al LDH (C, D, E), HRTEM image (F) of m-SiO_2@Co−Al LDH and EDX spectra (G) of m-SiO_2@Co−Al LDH.

mm^3 wrapped in an aluminum foil was exposed horizontally to a heat flux of 35 kW/m^2. Three parallel runs were performed for each sample to obtain averages. Microstructures of the char residues were studied by a JEOL JSM-2010 field-emission scanning electron microscopy (FESEM). Raman spectroscopy measurements were carried out with a SPEX-1403 laser Raman spectrometer (SPEX Co, U.S.A.) with excitation provided in backscattering geometry by a 514.5 nm argon laser line. Direct pyrolysis-mass spectrometry (DP-MS) analysis was performed with a Micromass GCT-MS spectrometer using the standard direct insertion probe for solid polymer materials, at a heating rate of 15 °C min^{-1} in the range 30−700 °C.

3. RESULT AND DISCUSSION

3.1. Characterization of m-SiO_2@Co−Al LDH. TEM image in Figure 1A shows that m-SiO_2 spheres are monodispersed with a uniform diameter of about 500 nm. Further magnification depicts that the mesochannels of the spheres are continuous throughout the shell with openings at surface and are radially oriented to the sphere surface (Figure 1B), which can absorb EP molecular chain. The surface of m-SiO_2 spheres is negatively charged as indicated by a ζ-potential of −45 mV. Hence, coating of the oppositely charged Co−Al LDH nanosheets via electrostatic interaction can easily occur

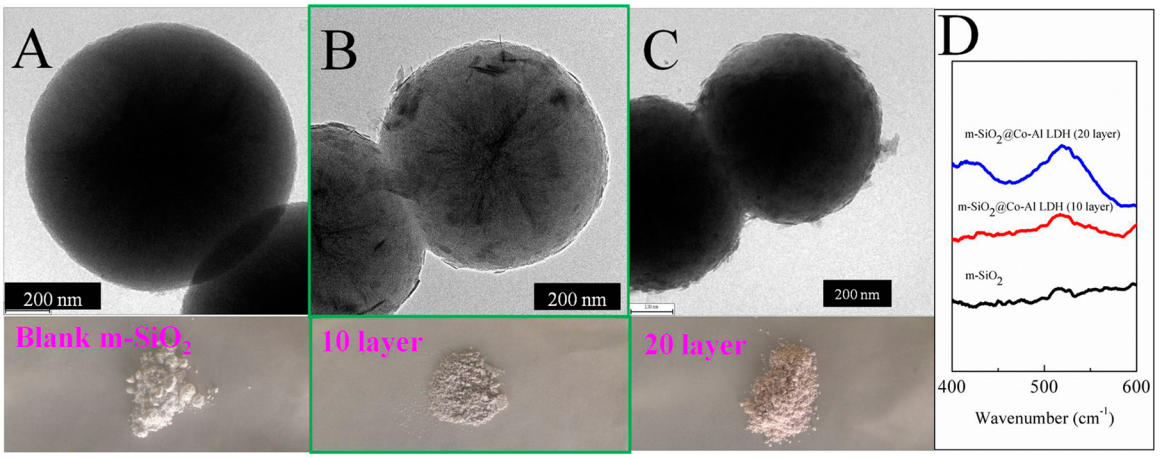

Figure 2. TEM images, digital photos (A, B, C) and UV−vis absorption spectra (D) of m-SiO_2, m-SiO_2@Co−Al LDH (10 layers) and m-SiO_2@Co−Al LDH (20 layers).

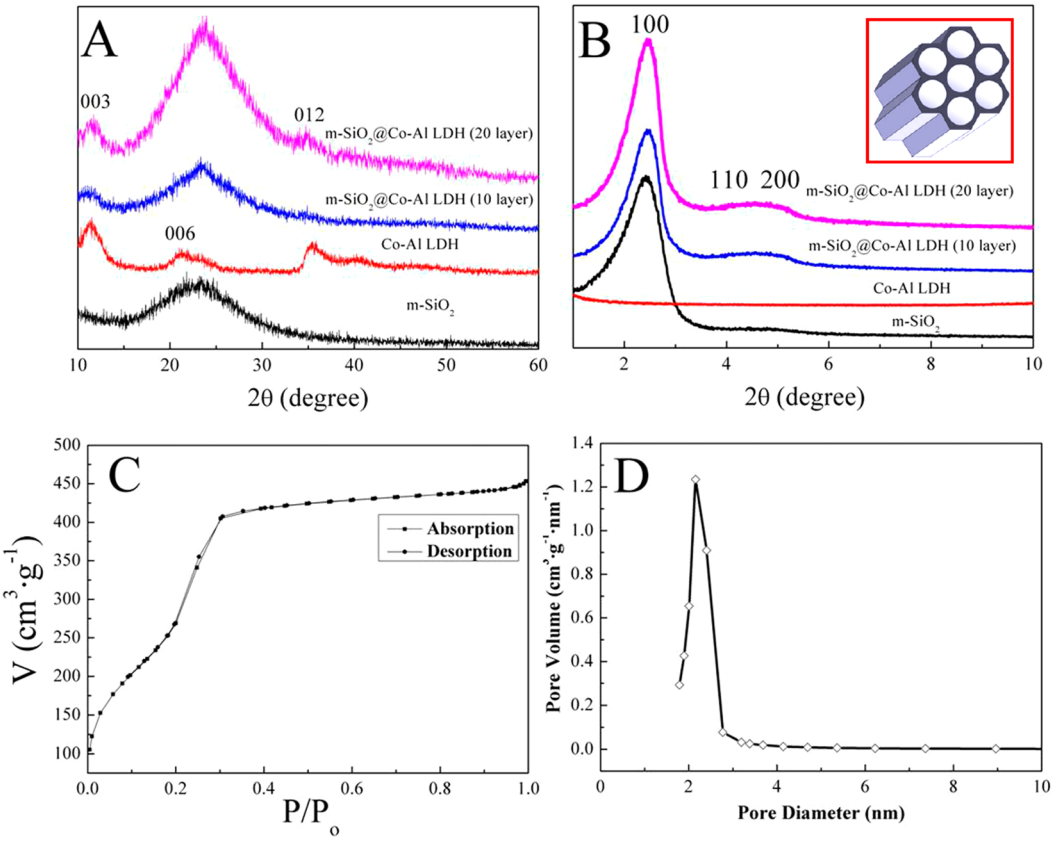

Figure 3. Wide-angle XRD pattern (A) and the small-angle XRD pattern (B) of m-SiO_2, Co−Al LDH, and m-SiO_2@Co−Al LDH, nitrogen sorption isotherm (C) and the pore size distribution curve (D) of m-SiO_2@Co−Al LDH. Inset in (B) is a structural model of the mesoporous silica shells, showing hexagonal symmetry.

without adding any additives or binding agents. The morphology of m-SiO_2@Co−Al LDH was further examined by TEM (Figures 2C, D, and E). It can be observed that the final sample consists of well dispersed spheres with an average diameter of around 550 nm. The surface of m-SiO_2 spheres (dark color) is coated with a layer of lighter colored LDH nanosheets. As shown in Figure 1F, the building block of nanosheets shows a repeating fringe of ∼0.8 nm, which are assembled with a face-to-face stacking to form a layer structure with a lateral scale of 8 nm. The ζ-potential of m-SiO_2@Co−Al LDH was measured to be +26.7 mV, further supporting that positively charged Co−Al LDH nanosheets have been effectively coated on the surface of m-SiO_2. The existence of Co−Al LDH coating on the surface of m-SiO_2 was also identified by EDX, as shown in Figure 1G.

As far as the layer number is concerned, the morphology of samples appears nearly same. For the blank m-SiO_2, the particles exhibit microspheres with a smooth surface (Figure 2A). With the layer number increased to 10, the spherical morphology of monodisperse m-SiO_2 spheres is preserved well after the deposition of nitrate LDH shell (Figure 2B). The only noticeable difference between the spheres with or without shells

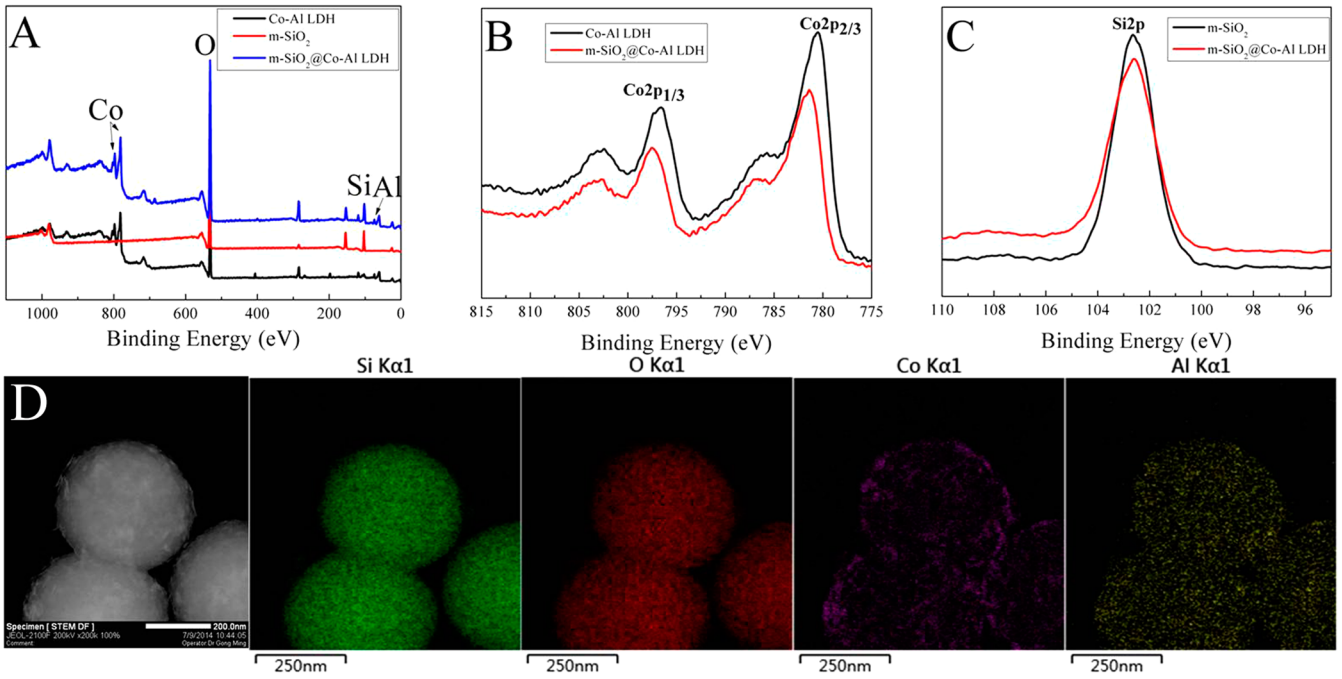

Figure 4. XPS survey spectra of Co–Al LDH, m-SiO_2, and m-SiO_2@Co–Al LDH (A), Co 2p XPS spectra of Co–Al LDH and m-SiO_2@Co–Al LDH (B), Si 2p XPS spectra of m-SiO_2 and m-SiO_2@Co–Al LDH (C), dark-field STEM image and elemental mapping of m-SiO_2@Co–Al LDH (D).

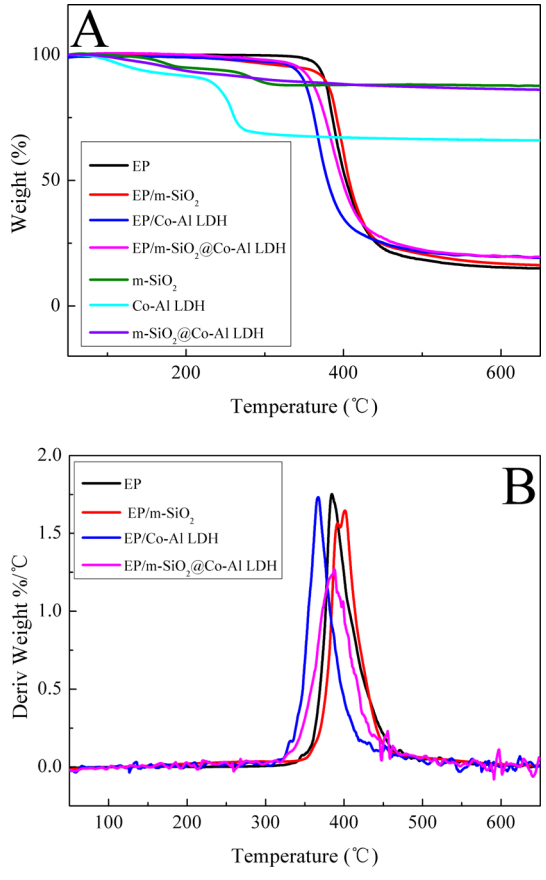

Figure 5. TGA (A) curves of m-SiO_2, Co–Al LDH, m-SiO_2@Co–Al LDH, pure EP and its nanocomposites and DTA curves of pure EP and its nanocomposites (B) in nitrogen.

Table 1. TGA Data for EP and Its Nanocomposites in Nitrogen

sample	$T_{-10\%}$ (°C)	$T_{-50\%}$ (°C)	T_{max} (°C)	char (%)
EP	376.0	403.2	385.2	14.7
EP/m-SiO_2	376.4	407.1	401.8	15.8
EP/Co–Al LDH	349.0	379.6	366.5	18.4
EP/m-SiO_2@Co–Al LDH	358.1	398.3	389.1	19.0

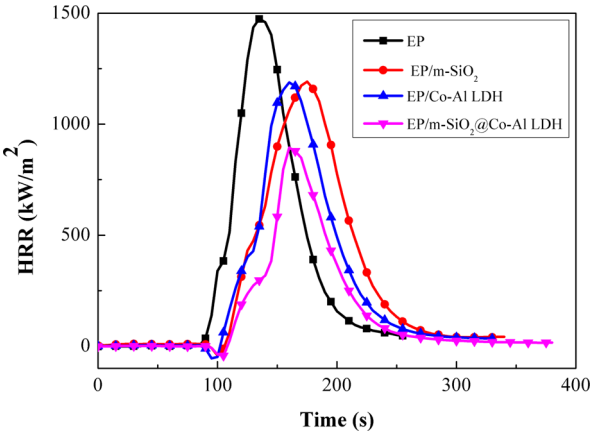

Figure 6. HRR curves of EP and its nanocomposites.

is the surface roughness. When the layer number is increased to 20, the surface of SiO_2 spheres is encapsulated with more LDH nanosheets and become coarser (Figure 2C). Moreover, there is an enhanced absorbance at λ = 525 nm (Figure 2D) with the increase of the layer number, which is in accordance with the color change of the samples.

The composition and structure of m-SiO_2, Co–Al LDH, and m-SiO_2@Co–Al LDH were identified by XRD, as shown in

Table 2. Cone Calorimeter Data of EP and Its Nanocomposites

sample	pHRR (kW/m^2)	THR (MJ/m^2)	EHC (MJ/kg)	MARHE (kW/m^2)	TSR (m^2/m^2)	char yield (%)
EP	1473.4	87.8	24.1	434.2	2734.9	5.2
EP/m-SiO_2	1191.2	96.5	26.4	383.8	2291.8	7.1
EP/Co−Al LDH	1188.1	84.3	23.8	421.6	2370.3	12.1
EP/m-SiO_2@Co−Al LDH	893.8	56.0	20.3	361.7	2085.2	20.7

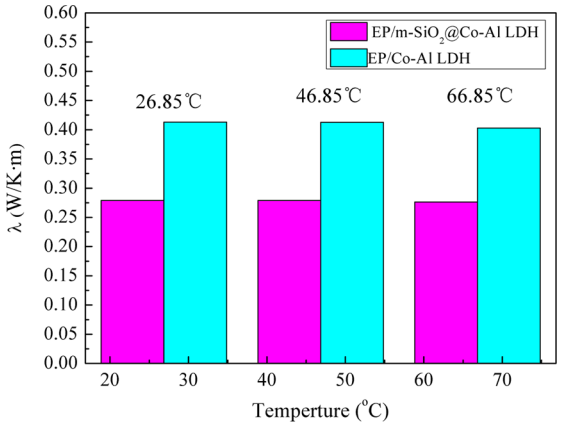

Figure 7. Thermal conductivity plot of the nanocomposites at different temperatures.

Figure 3. The wide-angle XRD pattern of m-SiO_2 exhibits a broad peak around 23°, revealing its amorphous nature.[28] For Co−Al LDH, all diffraction peaks can be indexed as Co−Al LDH.[29,30] The broadened diffraction peaks of Co−Al LDH indicate that the synthetic sample is composed of nanocrystals.[31] Comparing the m-SiO_2, Co−Al LDH, and m-SiO_2@Co−Al LDH wide-angle XRD patterns, two relatively weak peaks of m-SiO_2@Co−Al LDH at around 11.5° and 35.3° can be assigned to (003) and (012) of layered Co−Al LDH structure (Figure 3A). Moreover, the (006) peak of Co−Al LDH and the broad peak between 20° and 25° of m-SiO_2 were overlapping, so the broad peak of m-SiO_2 may cover the weak (006) peak of Co−Al LDH in the m-SiO_2@Co−Al LDH structure. The small-angle XRD diffraction of m-SiO_2 or m-SiO_2@Co−Al LDH exhibits a typical diffraction pattern of hexagonally packed mesopores (Figure 3B), implying their ordered mesostructure.[32] Nitrogen sorption isotherm of the m-SiO_2@Co−Al LDH spheres depicts a type IV curve according to the IUPAC nomenclature with a sharp capillary condensation step and a hysteresis loop in the p/p_0 range 0.2−0.4 (Figure 3C), indicating characteristics of mesoporous materials with narrow pore size distribution. The surface area and pore volume are calculated to be as high as about 1020 m^2 g^{-1} and 0.80 cm^3 g^{-1}. The detailed pore size distribution calculated on the basis of the nonlocal density functional theory exhibits the m-SiO_2@Co−Al LDH hybrids have micropores with a uniform size of around 1.2 nm (Figure 3D).

XPS analysis was used to study the surface composition and chemical state of the m-SiO_2, Co−Al LDH, and m-SiO_2@Co−Al LDH, which could provide information on the interaction between m-SiO_2 and Co−Al LDH. In Figure 4A, it can be found that the product contains Si, O, Co, and Al elements, indicating the formation of m-SiO_2@Co−Al LDH. The Co_{2p} spectrum is shown in Figure 4B. Two peaks of m-SiO_2@Co−Al

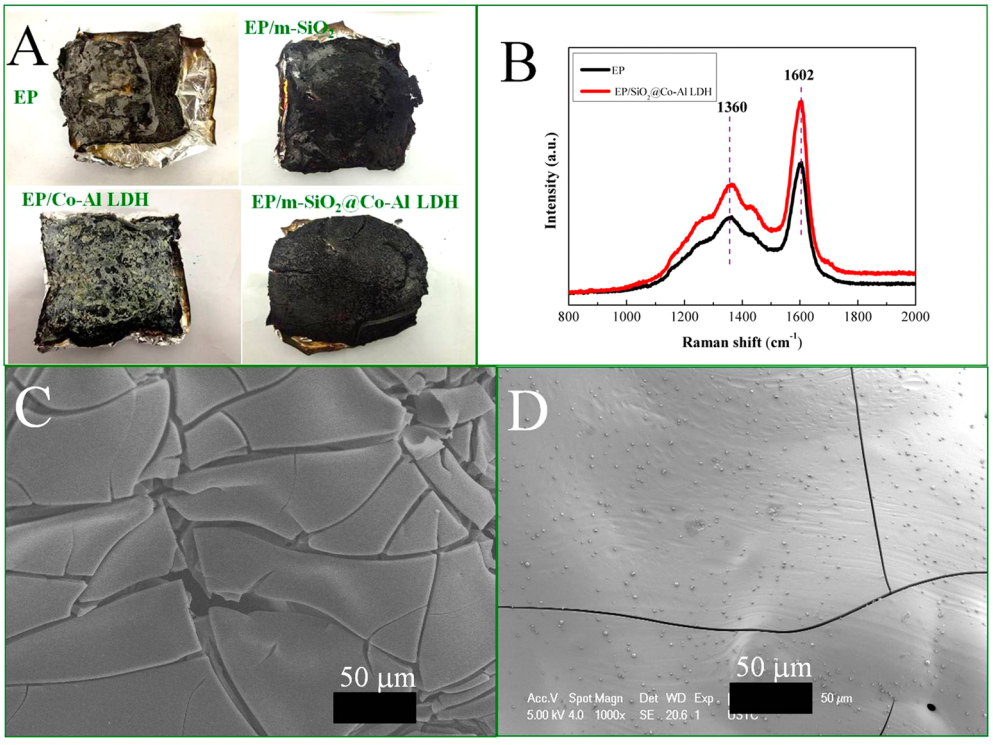

Figure 8. Digital photos (A) and Raman spectra (B) of the residues from EP and its nanocomposites, SEM images of residues of EP (C) and EP/m-SiO_2@Co−Al LDH (D).

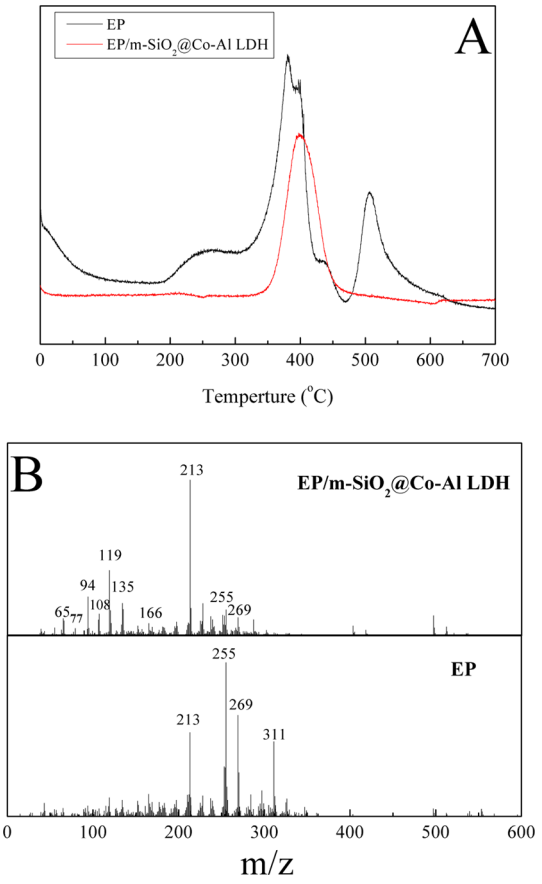

Figure 9. Total ion current (TIC) curves (A) of the decomposition process of EP and EP/m-SiO_2@Co−Al LDH, and EI-MS spectra (B) of compounds evolved from EP and EP/m-SiO_2@Co−Al LDH at the maximum of the peak in the TIC curves.

LDH are located at 781.2 and 796.8 eV, corresponding to Co $2p_{3/2}$ and Co $2p_{1/2}$. The Co $2p_{3/2}$ peak of m-SiO_2@Co−Al LDH appears at higher position than that of normal Co−Al LDH (Figure 4B), indicating a stronger interaction between silica shell and Co−Al LDH species.[33−35] The presence of m-SiO_2 can also be clearly confirmed from the Si 2p curve (Figure 4C). The position of 102.06 eV compares well with literature reports on binding energies for SiO_2. Furthermore, a dark-field scanning transmission electron microscopy (STEM) analysis of m-SiO_2@Co−Al LDH was performed to obtain more detailed information about the structure. As shown in Figure 4D, the dark-field STEM clearly demonstrates that the as-synthesized m-SiO_2@Co−Al LDH have a typical core−shell structure, and EDX element mapping of the same particles further shows the spatial distributions of Si, O, Co, and Al in nanoparticles of m-SiO_2@Co−Al LDH. The strong Si and O signal across the sphere confirms the m-SiO_2 core, while the Co and Al signals both detected in the surface region clearly suggests the adsorption of Co−Al LDH particles.

3.2. Thermal Stability of EP and Its Nanocomposites. The thermal stability of m-SiO_2, Co−Al LDH, m-SiO_2@Co−Al LDH, EP, and its nanocomposites was evaluated by TGA in nitrogen atmosphere. Figure 5 shows the TGA and derivative thermogravimetric (DTG) curves, and the corresponding data are given in Table 1. The temperatures at which 10% ($T_{-10\%}$), 50% ($T_{-50\%}$), and maximum (T_{max}) mass loss occurs are used as the measure of initial degradation temperature, half degradation temperature, and maximum degradation temperature, respectively. Pure m-SiO_2 shows a three-step thermogravimetric curve attributing to the loss of physically adsorbed water (room temperature−120 °C), the polycondensation of the silica network (120−210 °C) and the further condensation and dehydration of silanol groups (210−350 °C).[36−38] Co−Al LDH exhibits a three-step thermogravimetric profile accompanied a mass loss of about 34.3%, which should be due to surface-adsorbed water (from room temperature to 200 °C), chemisorbed water (200−350 °C), and the water arising from the dehydroxylation of the layers (225−500 °C).[19] In comparison, m-SiO_2@Co−Al LDH displays a consecutive mass loss with a weight loss of about 14.3%, implying that the integration of Co−Al LDH with m-SiO_2 obviously enhances the thermal stability of Co−Al LDH. From Figure 5 and Table 1, EP/m-SiO_2 nanocomposite is less thermally stable than pure EP when evaluated by $T_{-10\%}$, which is possibly attribute to the catalysis degradation initiated by silanol groups attached on m-SiO_2 as brønsted acid sites.[39] At higher temperatures, the EP molecular chains encapsulated by the silica walls shows high thermal stability due to the barrier effect of its porous structure, leading to a delayed degradation process of EP.[40] It is already known that transition metals including Co can cause catalytic degradation of polymer.[41] As expected, the Co−Al LDH incorporated results in an earlier degradation process of EP. Also, the introduction of m-SiO_2@Co−Al LDH leads to the decrease of degradation temperature, which is attributable to the earlier degradation of EP triggered by the catalytic activity of Co−Al LDH. However, compared to EP/Co−Al LDH, EP/m-SiO_2@Co−Al LDH nanocomposite presents the improved thermal stability owning to the barrier effect of m-SiO_2. As far as the char yield is concerned, the incorporation of Co−Al LDH or m-SiO_2@Co−Al LDH results in the improvement of the char residues at 700 °C, due to the catalytic carbonization effect of LDH.[42] Additionally, from the DTG profiles, the maximum mass loss rates (the peak of DTG curve) of EP/m-SiO_2 and EP/m-SiO_2@Co−Al LDH composites are much lower than that of neat EP, indicating that m-SiO_2 plays an effective mass-transport barrier role.

3.3. Fire Properties of EP and Its Composites. A cone calorimeter is a widely used tool for investigating combustion behaviors of materials.[43] Heat release rate (HRR) curves for EP and its composites are shown in Figure 6, and some important parameters obtained from cone calorimeter are listed in Table 2. With the incorporation of inorganic additives, the peak heat release rate (pHRR), total heat release (THR), effective heat of combustion (EHC), total smoke release (TSR), and maximum average heat rate emission (MAHRE) values are shifted to lower values except that the THR value of EP/m-SiO_2 increases. This phenomenon is attributed to the prolonged burning time that can be seen from the broad peak width in the pHRR curve and the formation of the combustible fragment from the catalytic degradation effect of m-SiO_2.[44−47] Compared to pure EP, the addition of m-SiO_2@Co−Al LDH brings about a 39.3% maximum decrease in pHRR, a 36.2% maximum decrease in THR, a 15.8% maximum decrease in EHC, a 23.8% maximum decrease in TSR, and a 16.7% maximum decrease in MAHRE. The results exhibit that the EP/m-SiO_2@Co−Al LDH nanocomposite presents the best flame retardancy among all the nanocomposites. According to the earlier literatures, m-SiO_2 has an interconnected porous structure with low thermal conductivity.[48] Heat and mass transport pathways in such a pore structure are long and tortuous, resulting in the diffusion of heat and the emission of volatile degradation products

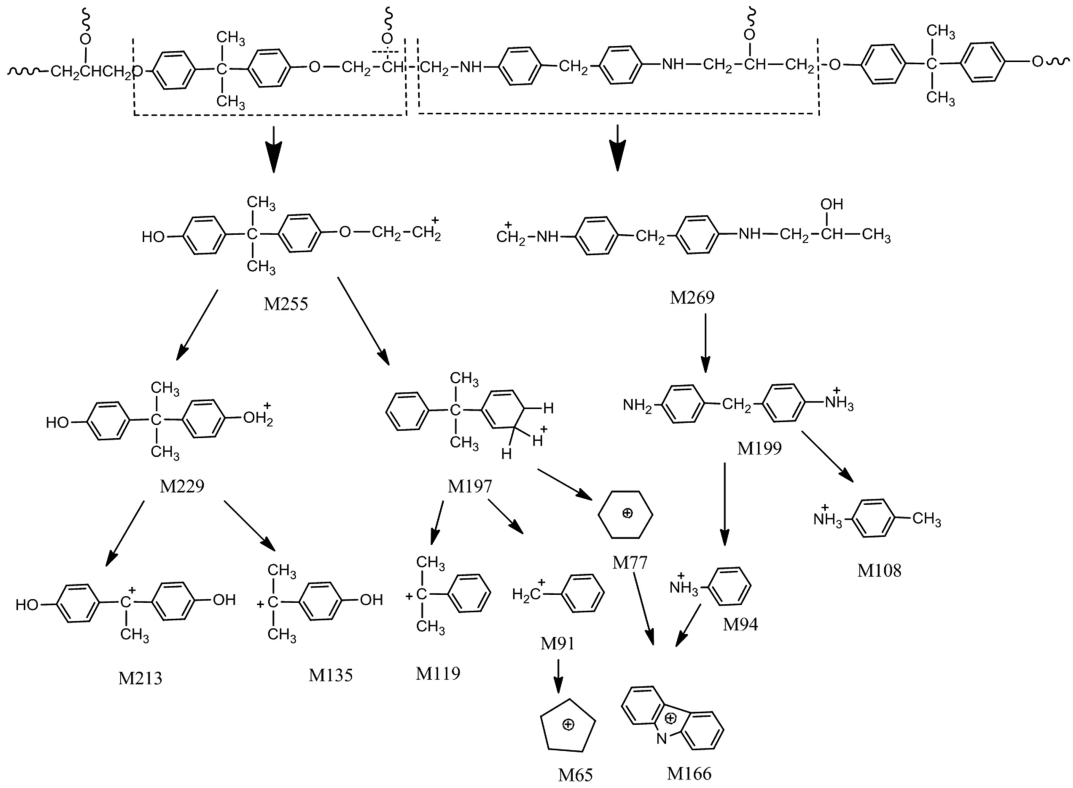

Figure 10. Simplified mass fragmentations of the EP/m-SiO_2@Co−Al LDH nanocomposite.

restricted. Thus, the labyrinth effects from m-SiO_2, containing mass barrier and thermal barrier effects, are speculated to be the primary reasons for the flame retardancy enhancement. The thermal barrier effect limits the permeation of heat; meanwhile, the mass barrier effect inhibits the escape of degradation products. In addition, the improved char yield of EP/m-SiO_2@Co−Al LDH on the basis of TGA results is another possible factor for the enhanced flame retardancy.

3.4. Flame Retardant Mechanism. To understand the flame-retardant mechanism, we studied the thermal conductivity, the char residues, and the degradation products of EP and its nanocomposites. Figure 7 shows the thermal conductivity of the nanocomposites at different temperatures. The thermal conductivity of EP/Co−Al LDH is around 0.4131 W/m·K, and it changes slightly with the increase of the temperature. As for the EP/m-SiO_2@Co−Al LDH nanocomposite, the thermal conductivity decreases compared to the EP/Co−Al LDH (0.4131 W/m·K) to 0.2789 W/m·K with a filler concentration of 2 wt %. It is suggested that heat diffusion was more difficult in the presence of m-SiO_2@Co−Al LDH. Combined with the Brunauer−Emmett−Teller (BET) results (Figures 3C and D), m-SiO_2@Co−Al LDH with larger surface area makes the path length longer that the transfer of oxygen and combustible products was inhibited, leading to retarded heat and mass release. Therefore, it is reasonable to believe that the low thermal conductivity and the labyrinth effect contributed by m-SiO_2@Co−Al LDH could lead to the better flame resistance.

Figure 8A shows images of the char residues after cone calorimeter test, in which there are little residues left after thermal degradation of pure EP. The incorporation of m-SiO_2@Co−Al LDH results in the significant improvement of the char yield, corresponding to the TGA results. To further explore the flame-retardant mechanism, Raman spectroscopy was utilized to characterize the structure and component of the residues. The Raman spectra of the residues of EP and EP/m-SiO_2@Co−Al LDH (Figure 8B) depict two bands at 1356 cm^{-1} (D-band) and 1591 cm^{-1} (G-band), which are associated with the vibration of the carbon atoms in disordered graphite or glassy carbons and the carbon atoms in crystalline graphite., respectively.[49] The present result indicates the formation of the graphitized char during EP combustion, due to the catalysis of m-SiO_2@Co−Al LDH.[50] As is well-known, the graphitized char is more conducive to suppress the diffusion of heat and mass during pyrolysis than disordered graphite or glassy carbons, which is ascribed to its higher thermal stability and compactness. Moreover, Figures 8C, D show the typical microstructure of the residues of EP and EP/m-SiO_2@Co−Al LDH nanocomposite. It is clearly found that a continuous and cohesive char surface is formed after the EP/m-SiO_2@Co−Al LDH nanocomposite combustion. The residue with a more cohesive and compact layer is beneficial for the inhibition of the heat, mass, and oxygen exchange, thereby improving the flame retardancy.

It is well-known that the pyrolysis products act as a key role in the flame-retardant performance of polymers. For the purpose of understanding the flame-retardant mechanism of the EP nanocomposites, the DP-MS tool was used to analyze the pyrolysis products. Figure 9 depicts the total ion current (TIC) chromatogram of EP and EP/m-SiO_2@Co−Al LDH nanocomposite, and EI-MS spectra corresponding to the TIC peaks with the maximum intensity. The pyrolysis fragment ions with the molecular weight of x are labeled as Mx and identified in Figure 10. For pure EP, the strong peak at 255 m/z corresponds to $C_{17}H_{19}O_2$. Also, the peaks at 269 m/z, 213 m/z, 197 m/z and 135 m/z can be assigned to the pyrolysis products of $C_{17}H_{21}N_2O$, $C_{14}H_{13}O_2$, $C_{15}H_{18}$, and $C_9H_{11}O$,

Additionally, some fragment ions can regroup to produce new products in high temperature. For instance, the benzene and aniline reconstitute to form carbazole (166 m/z), and the recombination between carbazole and benzene reconstitute a few polycyclic aromatic hydrocarbons (497 m/z). In contrast, the main fractions in the degradation products of the EP/m-SiO_2@Co−Al LDH include $C_{14}H_{13}O_2$ (213 m/z), which is with lower carbon numbers than that of neat EP. Actually, previous literatures reported that solid acids can catalyze the degradation of polymer, which results in the formation of pyrolysis products with lower carbon numbers, and the degradation products with lower carbon numbers could be easily catalyzed carbonization in the presence of metal oxides.[51,52] m-SiO_2 has been reported to be a most efficient solid acid for catalytic degradation of polymer due to the presence of many acid sites.[53,54] In this work, carbon numbers of pyrolysis products from the EP/m-SiO_2@Co−Al LDH composite is also decreased compared with that of EP. Thus, this undoubtedly results from the catalytic degradation effect for EP by m-SiO_2.[53,54] Also, degradation products with lower carbon numbers could extend contacting time of with metal oxides catalyst under the labyrinth effect of m-SiO_2. With different Co catalysts, Gong et al., used a simple method to synthesize carbon nanospheres through the carbonization of polystyrene.[55] Therefore, it is reasonable to believe that the enhanced flame resistant property for EP/m-SiO_2@Co−Al LDH is attributed to the synergism of m-SiO_2 and Co−Al LDH. In view of the results of the pyrolysis products, the mechanism for the improved fire resistant property of EP/m-SiO_2@Co−Al LDH nanocomposite is explained as follows. During the combustion process, m-SiO_2 with catalytic activity leads to the formation of pyrolysis products with lower carbon numbers, which can be easily catalyzed carbonization in the presence of metal oxides. Meanwhile, Co−Al LDH can catalyze carbonization of degradation products. Moreover, m-SiO_2 plays as a barrier that can absorb degraded products to extend contacting time of with metal compound catalyst. Furthermore, the degraded products are dehydrogenated and catalytically converted into char by the combination of m-SiO_2 labyrinth effect and Co−Al LDH catalysis effect.

4. CONCLUSIONS

In conclusion, m-SiO_2@Co−Al LDH spheres were synthesized by ultrasound assisted direct layered assembly of Co−Al LDH nanosheets on the surface of m-SiO_2 spheres, and its composition and structure was identified by XRD, BET, and XPS. The morphological characterization showed that, owning to the electric potential difference between m-SiO_2 and Co−Al LDH, m-SiO_2@Co−Al LDH exhibited that m-SiO_2 spheres were packaged by the Co−Al LDH nanosheets. Incorporation of 2 wt % m-SiO_2@Co−Al LDH into EP led to the increase of the char yield and the decrease of DTG peak value. Moreover, the pHRR, THR, EHC, TSR, and MAHRE values for EP/m-SiO_2@Co−Al LDH were obviously reduced. A plausible flame-retardant mechanism was hypothesized based on the analyses of thermal conductivity, char residue, and pyrolysis fragments. m-SiO_2 plays as a mass and heat barrier to prevent the diffusion of heat and the spread of the pyrolysis products and hence prolong the contact time between the pyrolysis products and the Co−Al LDH catalyst. The significant reduction of the fire hazard was primarily due to the synergistic action between the labyrinth effect of m-SiO_2 and the catalytic effect of Co−Al LDH.

AUTHOR INFORMATION

Corresponding Author

*Tel: 86 551 63601664. Fax: 86 551 63601664. Email: yuanhu@ustc.edu.cn.

Notes

The authors declare no competing financial interest.

ACKNOWLEDGMENTS

The work was financially supported by the National Natural Science Foundation of China (21374111), the National Basic Research Program of China (973 Program) (2012CB719701), and the National Key Technology R&D Program (2013BAJ01B05).

REFERENCES

(1) Corma, A. From Microporous to Mesoporous Molecular Sieve Materials and Their Use in Catalysis. *Chem. Rev.* **1997**, *97*, 2373−2419.

(2) Deng, Y. H.; Cai, Y.; Sun, Z. K.; Liu, J.; Liu, C.; Wei, J.; Li, W.; Liu, C.; Wang, Y.; Zhao, D. Y. Multifunctional Mesoporous Composite Microspheres with Well-Designed Nanostructure: A Highly Integrated Catalyst System. *J. Am. Chem. Soc.* **2010**, *132*, 8466−8473.

(3) Sun, Z. K.; Deng, Y. H.; Wei, J.; Gu, D.; Tu, B.; Zhao, D. Y. Hierarchically Ordered Macro-/Mesoporous Silica Monolith: Tuning Macropore Entrance Size for Size-Selective Adsorption of Proteins. *Chem. Mater.* **2011**, *23*, 2176−2184.

(4) Yang, H. F.; Shi, Q. H.; Tian, B. Z.; Xie, S. H.; Zhang, F. Q.; Yan, Y.; Tu, B.; Zhao, D. Y. A Fast Way for Preparing Crack-Free Mesostructured Silica Monolith. *Chem. Mater.* **2003**, *15*, 536−541.

(5) Park, S. C.; Ito, T.; Higgins, D. A. Single Molecule Tracking Studies of Flow-Aligned Mesoporous Silica Monoliths: Aging-Time Dependence of Pore Order. *J. Phys. Chem. B* **2013**, *117*, 4222−4230.

(6) Xue, C. F.; Wang, J. X.; Tu, B.; Zhao, D. Y. Hierarchically Porous Silica with Ordered Mesostructure from Confinement Self-Assembly in Skeleton Scaffolds. *Chem. Mater.* **2010**, *22*, 494−503.

(7) Suzuki, N.; Kiba, S.; Yamauchi, Y. Fabrication of Mesoporous Silica/Polymer Composites through Solvent Evaporation Process and Investigation of Their Excellent Low Thermal Expansion Property. *Phys. Chem. Chem. Phys.* **2011**, *13*, 4957−4962.

(8) Kiba, S.; Suzuki, N.; Okawauchi, Y.; Yamauchi, Y. Prototype of Low Thermal Expansion Materials: Fabrication of Mesoporous Silica/Polymer Composites with Densely Filled Polymer inside Mesopore Space. *Chem.—Asian J.* **2010**, *5*, 2100−2105.

(9) Nguyen, T. Q.; Wu, J. J.; Doan, V.; Schwartz, B. J.; Tolbert, S. H. Control of Energy Transfer in Oriented Conjugated Polymer−Mesoporous Silica Composites. *Science* **2000**, *288*, 652−656.

(10) Wang, S.; Liang, R.; Wang, B.; Zhang, C. Reinforcing Polymer Composites with Epoxide-Grafted Carbon Nanotubes. *Nanotechnology* **2008**, *19*, 085710.

(11) Liu, M. X.; Guo, B. C.; Du, M. L.; Lei, Y. D.; Jia, D. M. Natural Inorganic Nanotubes Reinforced Epoxy Resin Nanocomposites. *J. Polym. Res.* **2008**, *15*, 205−212.

(12) Koerner, H.; Hampton, E.; Dean, D.; Turgut, Z.; Drummy, L.; Mirau, P.; Vaia, R. Generating Triaxial Reinforced Epoxy/Montmorillonite Nanocomposites with Uniaxial Magnetic Fields. *Chem. Mater.* **2005**, *17*, 1990−1996.

(13) Abdalla, M.; Dean, D.; Theodore, M.; Fielding, J.; Nyairo, E.; Price, G. Magnetically Processed Carbon Nanotube/Epoxy Nanocomposites: Morphology, Thermal, and Mechanical Properties. *Polymer* **2010**, *51*, 1614−1620.

(14) Zhang, F. A.; Lee, D. K.; Pinnavaia, T. J. PMMA/Mesoporous Silica Nanocomposites: Effect of Framework Structure and Pore Size on Thermomechanical Properties. *Polym. Chem.* **2010**, *1*, 107−113.

(15) Qian, Y.; Wei, P.; Jiang, P. K.; Li, Z.; Yan, Y. G.; Ji, K. J. Aluminated Mesoporous Silica as Novel High-Effective Flame Retardant in Polylactide. *Compos. Sci. Technol.* **2013**, *82*, 1−7.

(16) Zhao, Y. F.; He, S.; Wei, M.; Evans, D. G.; Duan, X. Hierarchical Films of Layered Double Hydroxides by Using a Sol−Gel Process and Their High Adaptability in Water Treatment. *Chem. Commun.* **2010**, *46*, 3031−3033.
(17) Chen, C. P.; Gunawan, P.; Xu, R. Self-Assembled Fe_3O_4-Layered Double Hydroxide Colloidal Nanohybrids with Excellent Performance for Treatment of Organic Dyes in Water. *J. Mater. Chem.* **2011**, *21*, 1218−1225.
(18) Yu, X. Y.; Luo, T.; Jia, Y.; Xu, R. X.; Gao, C.; Zhang, Y. X.; Liu, J. H.; Huang, X. J. Three-Dimensional Hierarchical Flowerlike Mg/Al-Layered Double Hydroxides: Highly Efficient Adsorbents for As(V) and Cr(VI) Removal. *Nanoscale* **2012**, *4*, 3466−3474.
(19) Wang, X.; Zhou, S.; Xing, W. Y.; Yu, B.; Feng, X. M.; Song, L.; Hu, Y. Self-Assembly of Ni/Fe Layered Double Hydroxide/Graphene Hybrids for Reducing Fire Hazard in Epoxy Composites. *J. Mater. Chem. A* **2013**, *1*, 4383−4390.
(20) Shao, M. F.; Ning, F. Y.; Zhao, J. W.; Wei, M.; Evans, D. G.; Duan, X. Preparation of Fe_3O_4@SiO_2@Layered Double Hydroxide Core/Shell Microspheres for Magnetic Separation of Proteins. *J. Am. Chem. Soc.* **2012**, *134*, 1071−1077.
(21) Hu, J. L.; Yang, Q. H.; Lin, H.; Ye, Y. P.; He, Q.; Zhang, J. N.; Qian, H. S. Mesoporous Silica Nanospheres Decorated with CdS Nanocrystals for Enhanced Photocatalytic and Excellent Antibacterial Activities. *Nanoscale* **2013**, *5*, 6327−6332.
(22) Teng, Z. G.; Sun, C. H.; Su, X. D.; Liu, Y.; Tang, Y. X.; Zhao, Y. N.; Chen, G. T.; Yan, F.; Yang, N. N.; Wang, C. Y.; Lu, G. M. Superparamagnetic High-Magnetization Composite Spheres with Highly Aminated Ordered Mesoporous Silica Shell for Biomedical Applications. *J. Mater. Chem. B* **2013**, *1*, 4684−4691.
(23) Wu, Q. L.; Olafsen, A.; Vistad, O. B.; Roots, J.; Norby, P. Delamination and Restacking of a Layered Double Hydroxide with Nitrate as Counter Anion. *J. Mater. Chem.* **2005**, *15*, 4695−4700.
(24) Wang, L.; Wang, D.; Dong, X. Y.; Zhang, Z. J.; Pei, X. F.; Chen, X. J.; Chen, B. A.; Jin, J. A. Layered Assembly of Graphene Oxide and Co−Al Layered Double Hydroxide Nanosheets as Electrode Materials for Supercapacitors. *Chem. Commun.* **2011**, *47*, 3556−3558.
(25) Zhu, Y. F.; Shi, J. L.; Shen, W. H.; Dong, X. P.; Feng, J. W.; Ruan, M. L.; Li, Y. S. Stimuli-Responsive Controlled Drug Release from a Hollow Mesoporous Silica Sphere/Polyelectrolyte Multilayer Core/Shell Structure. *Angew. Chem., Int. Ed.* **2005**, *44*, 5083−5087.
(26) Bao, C. L.; Guo, Y. Q.; Song, L.; Kan, Y. C.; Qian, X. D.; Hu, Y. In Situ Preparation of Functionalized Graphene Oxide/Epoxy Nanocomposites with Effective Reinforcements. *J. Mater. Chem.* **2011**, *21*, 13290−13298.
(27) Das, G.; Karak, N. Thermostable and Flame Retardant *Mesua ferrea* L. Seed Oil Based Non-Halogenated Epoxy Resin/Clay Nanocomposites. *Prog. Org. Coat.* **2010**, *69*, 495−503.
(28) Yan, N.; Wang, F.; Zhong, H.; Li, Y.; Wang, Y.; Hu, L.; Chen, Q. W. Hollow Porous SiO_2 Nanocubes Towards High-performance Anodes for Lithium-Ion Batteries. *Sci. Rep.* **2013**, *3*, DOI: 10.1038/srep01568.
(29) Liu, Z. P.; Ma, R. Z.; Osada, M.; Iyi, N.; Ebina, Y.; Takada, K.; Sasaki, T. Synthesis, Anion Exchange, and Delamination of Co-Al Layered Double Hydroxide: Assembly of the Exfoliated Nanosheet/Polyanion Composite Films and Magneto-Optical Studies. *J. Am. Chem. Soc.* **2006**, *128*, 4872−4880.
(30) Zhang, W. F.; Ma, C.; Fang, J. H.; Cheng, J. P.; Zhang, X. B.; Dong, S. R.; Zhang, L. Asymmetric Electrochemical Capacitors with High Energy and Power Density Based on Graphene/Coal-LDH and Activated Carbon Electrodes. *RSC Adv.* **2013**, *3*, 2483−2490.
(31) Jiang, S. D.; Yao, Q. Z.; Zhou, G. T.; Fu, S. Q. Fabrication of Hydroxyapatite Hierarchical Hollow Microspheres and Potential Application in Water Treatment. *J. Phys. Chem. C* **2012**, *116*, 4484−4492.
(32) Kresge, C. T.; Leonowicz, M. E.; Roth, W. J.; Vartuli, J. C.; Beck, J. S. Ordered Mesoporous Molecular-Sieves Synthesized by a Liquid-Crystal Template Mechanism. *Nature* **1992**, *359*, 710−712.
(33) Yan, N.; Chen, Q. W.; Wang, F.; Wang, Y.; Zhong, H.; Hua, L. High Catalytic Activity for CO Oxidation of Co_3O_4 Nanoparticles in SiO_2 Nanocapsules. *J. Mater. Chem. A* **2013**, *1*, 637−643.
(34) Fan, G. L.; Wang, H.; Xiang, X.; Li, F. Co−Al Mixed Metal Oxides/Carbon Nanotubes Nanocomposite Prepared via a Precursor Route and Enhanced Catalytic Property. *J. Solid State Chem.* **2013**, *197*, 14−22.
(35) Li, J.; Tang, S. B.; Lu, L.; Zeng, H. C. Preparation of Nanocomposites of Metals, Metal Oxides, and CarbonNanotubes via Self-Assembly. *J. Am. Chem. Soc.* **2007**, *129*, 9401−9409.
(36) Shi, J. Y.; Yao, Q. Z.; Li, X. M.; Zhou, G. T.; Fu, S. Q. Formation of Asymmetrical Structured Silica Controlled by a Phase Separation Process and Implication for Biosilicification. *PLoS One* **2013**, *8*, e61164.
(37) Lin, H. Y.; Chen, Y. W. Preparation of Spherical Hexagonal Mesoporous Silica. *J. Porous Mater.* **2005**, *12*, 95−105.
(38) Hukkamaki, J.; Pakkanen, T. T. Amorphous Silica Materials Prepared by Neutral Templating Route Using Amine-Terminated Templates. *Microporous Mesoporous Mater.* **2003**, *65*, 189−196.
(39) Tsutsumi, K.; Kurata, N.; Takata, E.; Furuichi, K.; Nagano, M.; Tabata, K. Silicon Semiconductor-Assisted Bronsted Acid-Catalyzed Dehydration: Highly Selective Synthesis of 5-Hydroxymethylfurfural from Fructose under Visible Light Irradiation. *Appl. Catal., B* **2014**, *147*, 1009−1014.
(40) Yan, X. Q.; Wang, X. J.; Tang, Y.; Ma, G. C.; Zou, S. H.; Li, R. H.; Peng, X. G.; Dai, S.; Fan, J. Unusual Loading-Dependent Sintering-Resistant Properties of Gold Nanoparticles Supported within Extra-Large Mesopores. *Chem. Mater.* **2013**, *25*, 1556−1563.
(41) Wang, D. Y.; Das, A.; Costa, F. R.; Leuteritz, A.; Wang, Y. Z.; Wagenknecht, U.; Heinrich, G. Synthesis of Organo Cobalt Aluminum Layered Double Hydroxide via a Novel Single-Step Self-Assembling Method and Its Use as Flame Retardant Nanofiller in PP. *Langmuir* **2010**, *26*, 14162−14169.
(42) Hong, N. N.; Song, L.; Wang, B. B.; Stec, A. A.; Hull, T. R.; Zhan, J.; Hu, Y. Co-Precipitation Synthesis of Reduced Graphene Oxide/NiAl-Layered Double Hydroxide Hybrid and Its Application in Flame Retarding Poly(Methyl Methacrylate). *Mater. Res. Bull.* **2014**, *49*, 657−664.
(43) Cheng, K. C.; Yu, C. B.; Guo, W. J.; Wang, S. F.; Chuang, T. H.; Lin, Y. H. Thermal Properties and Flammability of Polylactide Nanocomposites with Aluminum Trihydrate and Organoclay. *Carbohydr. Polym.* **2012**, *87*, 1119−1123.
(44) Laufer, G.; Kirkland, C.; Cain, A. A.; Grunlan, J. C. Clay−Chitosan Nanobrick Walls: Completely Renewable Gas Barrier and Flame-Retardant Nanocoatings. *ACS Appl. Mater. Interfaces* **2012**, *4*, 1643−1649.
(45) Kashiwagi, T.; Grulke, E.; Hilding, J.; Groth, K.; Harris, R.; Butler, K.; Shields, J.; Kharchenko, S.; Douglas, J. Thermal and Flammability Properties of Polypropylene/Carbon Nanotube Nanocomposites. *Polymer* **2004**, *45*, 4227−4239.
(46) Qian, X. D.; Yu, B.; Bao, C. L.; Song, L.; Wang, B. B.; Xing, W. Y.; Hu, Y.; Yuen, R. K. K. Silicon Nanoparticle Decorated Graphene Composites: Preparation and Their Reinforcement on the Fire Safety and Mechanical Properties of Polyurea. *J. Mater. Chem. A* **2013**, *1*, 9827−9836.
(47) Cain, A. A.; Nolen, C. R.; Li, Y. C.; Davis, R.; Grunlan, J. C. Phosphorous-Filled Nanobrick Wall Multilayer Thin Film Eliminates Polyurethane Melt Dripping and Reduces Heat Release Associated with Fire. *Polym. Degrad. Stab.* **2013**, *98*, 2645−2652.
(48) Hoffmann, F.; Cornelius, M.; Morell, J.; Froba, M. Silica-Based Mesoporous Organic−Inorganic Hybrid Materials. *Angew. Chem., Int. Ed.* **2006**, *45*, 3216−3251.
(49) Fang, M.; Wang, K. G.; Lu, H. B.; Yang, Y. L.; Nutt, S. Single-Layer Graphene Nanosheets with Controlled Grafting of Polymer Chains. *J. Mater. Chem.* **2010**, *20*, 1982−1992.
(50) Lespade, P.; Aljishi, R.; Dresselhaus, M. S. Model for Raman-Scattering from Incompletely Graphitized Carbons. *Carbon* **1982**, *20*, 427−431.

(51) Song, R. J.; Jiang, Z. W.; Bi, W. G.; Cheng, W. X.; Lu, J.; Huang, B. T.; Tang, T. The Combined Catalytic Action of Solid Acids with Nickel for the Transformation of Polypropylene into Carbon Nanotubes by Pyrolysis. *Chem.—Eur. J.* **2007**, *13*, 3234−3240.
(52) Song, R. J.; Jiang, Z. W.; Yu, H. O.; Liu, J.; Zhang, Z. J.; Wang, Q. W.; Tang, T. Strengthening Carbon Deposition of Polyolefin Using Combined Catalyst as a General Method for Improving Fire Retardancy. *Macromol. Rapid Commun.* **2008**, *29*, 789−793.
(53) Eren, E.; Guney, M.; Eren, B.; Gumus, H. Performance of Layered Birnessite-Type Manganese Oxide in the Thermal-Catalytic Degradation of Polyamide 6. *Appl. Catal., B* **2013**, *132*, 370−378.
(54) Karami, C.; Ahmadian, H.; Nouri, M.; Jamshidi, F.; Mohammadi, H.; Ghodrati, K.; Farrokhi, A.; Hamidi, Z. A Novel Method for Synthesis of Cobalt Manganese Oxide Nanocatalysts as a Recyclable Catalyst for the Synthesis of Some Bis(Indolyl) Methane Derivatives. *Catal. Commun.* **2012**, *27*, 92−96.
(55) Gong, J.; Liu, J.; Chen, X. C.; Wen, X.; Jiang, Z. W.; Mijowska, E.; Wang, Y. H.; Tang, T. Synthesis, Characterization, and Growth Mechanism of Mesoporous Hollow Carbon Nanospheres by Catalytic Carbonization of Polystyrene. *Microporous Mesoporous Mater.* **2013**, *176*, 31−40.